JOURNAL OF SPACECRAFT AND ROCKETS
Vol. 40, No. 6, November–December 2003

Spacecraft Charging for Microsatellite KITSAT-3

H. J. Kim,* J. J. Lee,† J. G. Rhee,* E. S. Lee,† K. W. Min,‡ and D. K. Sung§
Korea Advanced Institute of Science and Technology, Daejon 305-701, Republic of Korea
and
J. Seon,¶ Y. H. Jung,** and S. D. Park††
SaTReC Initiative Co., Ltd., Daejon 302-120, Republic of Korea

Floating potentials for a microsatellite KITSAT-3 are measured with an electron temperature probe. The orbit of the satellite is 730-km altitude, sun-synchronous, with a fixed local time of descending node near 1200 hrs local time. The dimension of the satellite in stowed configuration is approximately $495 \times 614 \times 852$ mm^3. The weight of the satellite is 112 kg. In the dayside, a series of attitude maneuvering is performed to rotate the satellite. Significant correlation between the currents generated from the solar arrays and the floating potentials is found. The initial floating potentials that are largely negative (<-10 V) when the solar arrays are directed toward the sun are found to increase up to ~ -3 V as the rotation of the spacecraft brings the solar arrays nearly perpendicular to the sunlight. The result of the potential variation is verified by a numerical simulation with NASCAP/LEO. The present investigation finds that the floating potentials for a microsatellite KITSAT-3 are determined by the negative charging of the satellite due to the presence of solar arrays.

Nomenclature

A_C	=	conductive area of the satellite body, m^2
A_S	=	surface area of the satellite, m^2
A_W	=	conductive area of interconnectors, m^2
B	=	magnetic field, nT
e	=	electron charge, 1.60×10^{-19} C
I	=	current, A
I_{SC}	=	current collected in the ram direction by the orbital motion of the satellite, A
I_{TH}	=	current collected due to the satellite potential, A
k	=	Boltzmann constant
q	=	charge, C
V_p	=	satellite potential, V
V_{pp}	=	peak-to-peak voltage, V
V_{sc}	=	orbital speed of satellite, m/s
α	=	angle between the orbital velocity and the normal vector of the conductive surface
$\Delta\Phi$	=	potential difference between the solar cells, V
θ	=	angle of satellite orientation relative to the orbital velocity, deg

Introduction

THE charging of spacecraft relative to the ambient plasmas has been previously investigated for both the geosynchronous satellites and low-Earth-orbiting satellites. (See Hastings and Garrett[1] and references therein.) The interpretation of these phenomena based on plasma theories from laboratory[2] has been successfully applied for space observations. The imbalance of electrical currents between the incident electrons and ions generally gives a floating potential to the spacecraft relative to the ambient plasmas. It has been found that additional effects such as photoionization of the spacecraft surface or scattering of ion species from the surface also have to be taken into account for proper determination of the potentials.

Modern spacecraft deploy large arrays of solar cells for the generation of electrical power. This deployment of solar arrays provides a potential difference between the solar arrays and main structure of the spacecraft, to which the negative end of the solar arrays is usually connected. This potential gradient can modify the trajectories of incident charged particles and, in turn, modify the floating potentials of the spacecraft. For example, floating potentials comparable to the solar array have been found for the Space Flyer Unit (SFU)[3] and have been predicted for the International Space Station (ISS).[4] The consequence of such a presence of a large potential difference due to the solar arrays has been further investigated.[5] However, these findings are for large space structures, where the fundamental scale length of the physical system, such as ion gyroradius, is significantly smaller than the characteristic length of the structure. The purpose of this paper is to report variations of floating potentials for a microsatellite whose physical dimension is usually significantly smaller than previously examined satellites. A brief introduction to KITSAT-3 and its instrumentation is given. Observations of floating potentials that are obtained with the instrument are provided, and discussions of the observations are given.

KITSAT-3 and Science Payloads

KITSAT-3

KITSAT-3 was launched on 26 May 1999 by the Indian PSLV-C2 launcher as a piggyback payload, along with the Indian IRS-P4 and the German DLR-TUBSAT, into a 730-km sun-synchronous orbit. The orbit of KITSAT-3 has a fixed descending node at local time near 1200 hrs. The microsatellite has been operating successfully and has produced imagery of Earth's surfaces in several visible spectral bands. The main objective of the KITSAT-3 program is to develop and operate an advanced microsatellite system. KITSAT-3 was designed by the use of the knowledge and experience acquired from the previous KITSAT-1 and 2 programs. Figure 1 shows the configuration of the satellite. The specifications of the satellite and key features such as deployable solar arrays with Ga/As cells, 8-Gbit solid-state mass memory systems and X-band transmission for image down loading, are summarized in Tables 1 and 2. There are three solar arrays for KITSAT-3, two deployable and one body fixed. Each panel has six strings of 49 solar cells. The 49 solar cells are connected in a series in the string. Each string is connected to the neighboring strings in parallel. Because the output current of each solar cell is near 0.24 A at 0.85 V, the solar arrays generate about 180 W under full illumination.

Received 16 May 2001; revision received 1 December 2002; accepted for publication 25 February 2003.

*Graduate Research Assistant, Department of Physics.
†Scientist, Department of Physics.
‡Professor, Department of Physics.
§Professor, Department of Electrical Engineering.
¶Director, Research and Development Center; jhseon@satreci.com.
**Senior Engineer, Space Systems Division.
††Managing Director.

Table 1 Specifications of KITSAT-3

Classification	Specifications
Dimension	$495 \times 614 \times 852$ mm^3 (stowed)
	$495 \times 1497 \times 819$ mm^3 (deployed)
Attitude control	Three-axis stabilized
Frequency bands	Uplink: VHF
	Downlink: UHF, *S*/*X* band
Main computer	Intel i80960
Payloads	Multispectral Earth imaging system
	SENSE
	REME
	HEPT
	ETP
	SMAG
Pointing accuracy	<0.5 deg
Power	150 W (at end of life) from deployed solar arrays
	output voltages
	+28 V (unregulated), ±12 V, +5 V (regulated)
Weight	112 kg

Table 2 Key features of KITSAT-3

Subsystem	Key features
Attitude determination	Three-axis stabilization based on four reaction wheels
Control subsystem	Pointing accuracy: <0.5 deg (2σ)
	Stability: 0.014 deg/s
	Pointing knowledge: 1 arcmin (1σ)
Electrical power subsystem	GaAs/Ge solar cells on honeycomb substrate
	NiCd batteries (8 Ah)
	PPT approach
	Solar power >150 W at EOL
Command and data handling	Two onboard computers (32/16 bits)
	Modular telemetry control network
	Data network: 38.4 kbps
	Analog telemetry channels: up to 192
	Digital telemetry channels: up to 114
RF subsystem	9600 bps/1200 bps VHF telemetry tracking and communication uplink
	38.4 kbps/9600 bps/1200 bps UHF and *S*-band telemetry tracking and communication downlink
Structure and thermal	Modular structure
	Aluminum honeycomb panels
	Passive thermal control design

Science Payloads Aboard KITSAT-3

In addition to the Earth imaging payload, the microsatellite is implemented with the Space Environment Scientific Experiment (SENSE) that is developed for in situ measurements of the space environment.[6] The SENSE consists of four instruments: the high-energy particle telescope (HEPT), radiation effects on microelectronics (REME), electron temperature probe (ETP), and scientific magnetometer (SMAG). HEPT measures the energy of electrons, protons, and alpha particles in the 0.25–60-MeV range. The instrument also determines the incident angle of incoming particles. REME monitors the effects of radiation on microelectronics using a dosimeter. SMAG is a magnetometer improved from the one used for attitude determination. The flux gate type sensor is positioned outside the satellite to reduce magnetic field disturbance caused by the satellite electronics.

ETP is designed to measure the densities and temperatures of the cold, ionospheric electrons. The instrument consists of two 12-cm-diam disks separated by 2 cm (Fig. 2). The surfaces of the probes are gold coated. One of the probes (probe a in Fig. 2) is driven with sinusoidal variations of voltages of 0 V, $0.4V_{pp} \pm 30$ mV, and $0.8V_{pp} \pm 30$ mV at 30-kHz frequencies, whereas no variation is applied to probe b. The probes are electrically isolated from the spacecraft ground because each probe is connected to the ground through a 100-MΩ resistor. The dc component variations of the probe potentials due to the applied voltages are then measured to estimate the electron temperatures. The measured voltages from probes a and b are then used to estimate the electron temperatures and floating potentials of the satellite, respectively. The sampling rate of the instrument is 20/s. For the present study, only the floating potential of the probe relative to the satellite conductive body structure is measured with the ETP because of the limited operation of the instrument. The electron temperature is not available. Note that the measured probe potential is approximately the same as the floating potential if the probe current across the 100-MΩ resistor is less than the ion saturation current of the Langmuir probe theory. For the ram side of the spacecraft, the expected ion saturation current, $\sim 10^{-4}$ A, is large enough to allow an interpretation of the probe potential as floating potential. However, in the wake side, the floating potential can significantly deviate from those of the ram side to collect sufficient currents. This temperature probe on KITSAT-3 is similar to those previously flown on other satellites such as Akebono and Ohzora.[7]

Observation

On 12 January 2000, a rotation of KITSAT-3 was performed when the satellites were located in the Earth's dayside. Figure 3 shows, from top to bottom, the variations of floating potentials of the satellite, voltages, currents, and powers generated from the solar arrays, respectively. The universal time (UT) and latitude of the satellite for which each potential is measured are summarized along the abscissa. The satellite is initially directed for maximal power generation (attitude A in Fig. 4). The normal vector of the solar array is directed southward by about 20 deg off of the equatorial plane. From 0800 hrs UT, a series of attitude maneuvering is performed. Each maneuvering corresponds to a 90-deg rotation in the noon–midnight plane from the preceding attitude. The rotation is performed at an angular speed of about 0.7 deg/s and takes about 130 s for completion. The duration between the successive operations is 150 s. The duration for each rotation is designated with circled number in Fig. 4 and Table 3. The approximate attitudes corresponding to the beginning and end of each rotation are represented in letters and are summarized in Table 3. The geographical longitudes and latitudes, as well as UT, are also shown.

The first rotation approximately aligns the normal vector perpendicular to the sunlight and toward the northern hemisphere (attitude B), the second rotation toward the nightside (attitude C), and the third rotation perpendicular to the sunlight again, but toward the southern hemisphere (attitude D). The attitudes and angular positions of the satellites during the rotations are summarized in Fig. 4. The angles of the solar arrays to the sun and to the ram direction are given in Table 3. The definition of the axis and angles are found in the upper-left-hand corner of Fig. 4.

Note that the floating potential is −10 V before 0800 hrs and after 0810 hrs UT. This is because the maximum magnitudes of floating potential that ETP can measure are 10 V. Therefore, any potential smaller than −10 V (magnitudes greater than 10 V) is detected at the saturation voltage. The satellite performs a 90-deg rotation at 0800 UT. The floating potential remains at −10 V until about 0801 UT, presumably because of the saturation of the instrument, but eventually increases above −10 V. The maximum floating potential is about −3.7 V near 0803 UT. The floating potential begins to decrease again as the satellite is further rotated toward the Earth. Considerable enhancement in the generated power and current is found when the satellite completes the second 90-deg rotation (attitude C). It is likely that this enhancement of the currents is due to the reflected sunlight from the Earth (albedo). Then the satellite is maneuvered away from the Earth and further directed toward the southern hemisphere (attitude D). The currents again decrease. The voltages and currents resume their initial magnitudes as the satellite completes a whole rotation from attitude D to E. The array voltage does not go to zero in configurations B and D because the system battery is always connected to the arrays.

Note that smaller magnitudes for the potentials are found near the completion of the satellite maneuvering 3 (from C to D) in Fig. 4. During about 0806:44–0806:58 UT, the potentials temporarily increase to about −8 V above the saturation voltage. This

Table 3 Angular locations of KITSAT-3

Attitude	Time, UT	Latitude,°	Longitude,°	Angle of solar arrays to sun, ϑ_{SS}, deg	Angle of solar arrays to ram, ϑ_{SR}, deg
A	0800:00	13.3	296.0	11.3	−51.7
B	0802:30	4.3	298.0	88.3	−114.7
C	0805:00	−4.7	300.0	168.7	146.3
D	0807:30	−13.7	302.2	268.4	47.3
E	0810:00	−22.6	303.9	11.3	−24.3

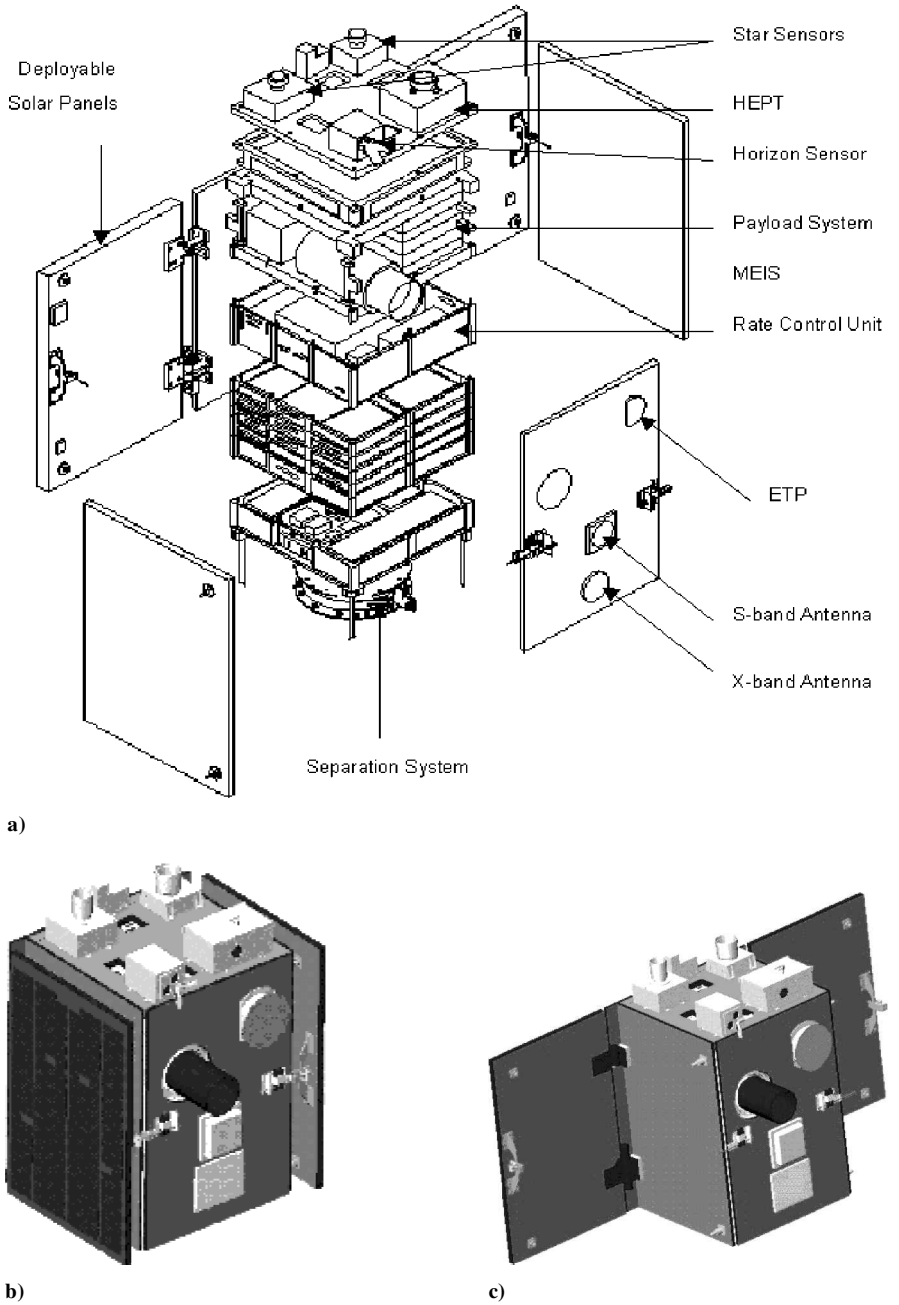

Fig. 1 Structural configuration of KITSAT-3 Satellite: a) external view, b) stowed configuration, and c) deployed configuration.

increase of the potential is likely because a considerably smaller amount of current (≈ 0.2 A) is generated from the solar arrays because the arrays do not face either the sunlight or the albedo near attitude D. No negative charging of the satellite would be necessary if the solar arrays do not generate electrical power. However, the measurement of currents and attitudes of the satellite is acquired only once every minute in the present study. This limitation on the measurement does not allow a clear explanation of the variations of the floating potential during 0806:44–0806:58 UT.

Discussion

It is found that the floating potential of the satellite is below −10 V when the solar arrays are directed toward the sun for maximal power generation. On the other hand, the potential rapidly increases if the generated voltages and currents become smaller due to the rotation

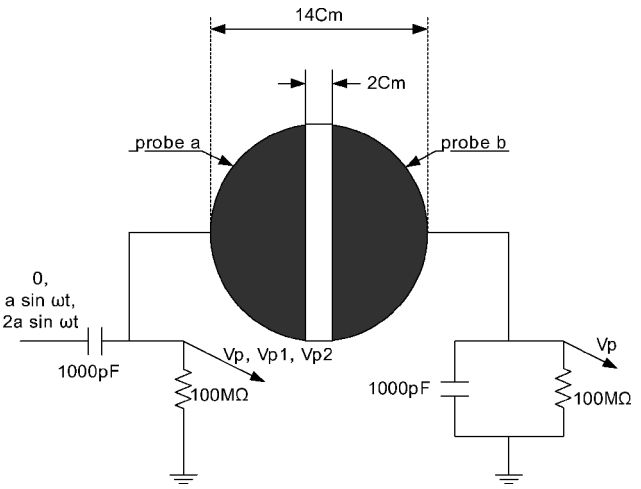

Fig. 2 Functional block diagram of the electron temperature probe aboard KITSAT-3.

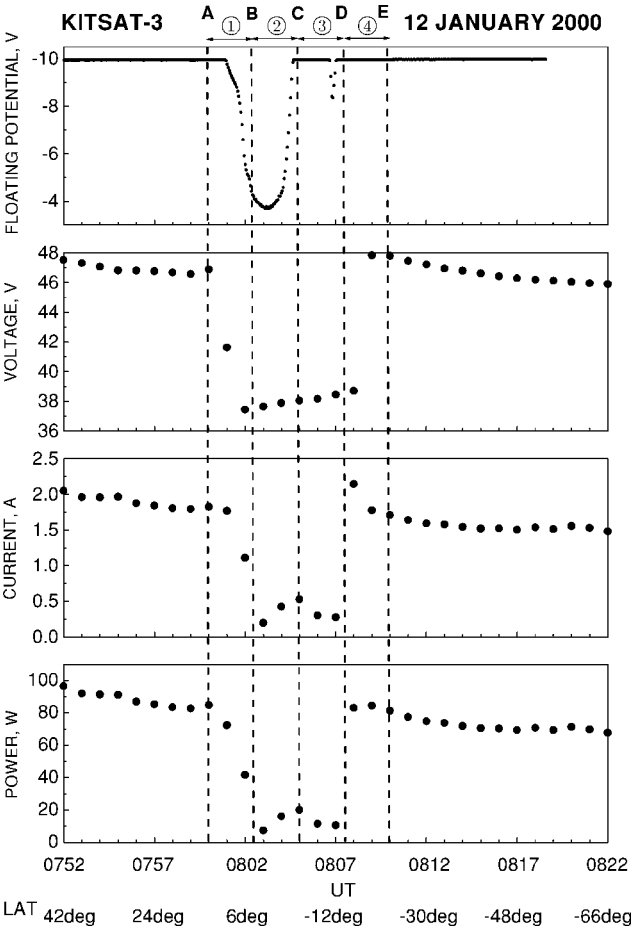

Fig. 3 Variations of floating potentials for KITSAT-3 when the satellite is rotated on the dayside of the Earth.

of the satellite away from the sun. This correlation between the floating potential and the generated power from the solar arrays suggests that the observed potential variation is due to the electrical biasing of the satellite by the solar arrays. Similar effects for large spacecraft were previously investigated.[3,4]

To compare quantitatively with the measurements, a numerical analysis is performed for KITSAT-3 with NASCAP/LEO.[8] NASCAP/LEO takes into account the three-dimensional geometry of the satellite and solves the Poisson and Boltzmann equation to determine the floating potentials. The basic assumption underlying NASCAP/LEO current calculations is that plasma currents may

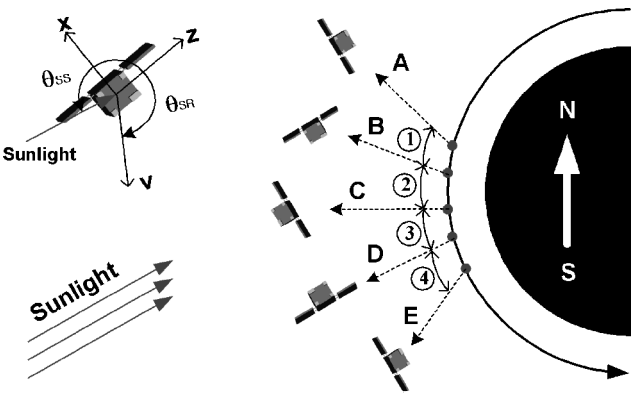

Fig. 4 Rotation of KITSAT-3 during 0800–0810 UT on 12 January 2000.

be considered to originate at a well-defined sheath boundary. The boundary represents a sharp demarcation between a low potential exterior region containing neutral undisturbed plasma and a high potential interior region from which one species (ions for positive potentials and electrons for negative potentials) is excluded. The other species diffuses across the sheath boundary at a rate given by the thermal currents. The charged particles constituting this current undergo motion consistent with the electric and magnetic fields inside the sheath. The space charge is calculated by a function that interpolates between Debye screening at low potentials to an accelerated distribution with particle convergence at high potentials.

For the calculation of electrostatic potential, a thin sheath approximation is first made to acquire an initial guess for the spacecraft ground potential. Then, it assigns either a fixed potential or electric field boundary condition to each insulating surface cell and calculates the mean potential of composite solar array surface cells. Calculation of the electrostatic potential about the spacecraft is made to obtain the sheath currents to the spacecraft. The ambient current to low potential surfaces is added to the sheath current to give the total current to the spacecraft. The accumulated information is used to generate a revised estimate of the spacecraft ground potential. This procedure is repeated until a converged answer is obtained.[9] The potentials of the solar arrays are obtained by application of the SOLAR and FLOAT modules of NASCAP/LEO. There are eight conductors in the simulation. Two conductors were used for the body of satellite, whereas six conductors were used for the arrays.

Figure 5 shows the numerical model of KITSAT-3 and the definition of axis in the simulation. The majority of the satellite is covered with a tape that consists of a Kapton® layer, a vacuum deposited aluminum layer, and an acrylic pressure-sensitive adhesive tape. The Kapton side of the tape faces the space. The top and bottom surfaces ($+Y$ and $-Y$ directions, respectively) are covered with aluminum foil for thermal considerations. The aluminum foil provides an electrical connection of the surfaces with the satellite. The solar array ($+X$ direction) is modeled with silicon solar cells. The direction and origin of each axis are also illustrated in Fig. 5a. The size of the satellite in stowed configuration for the simulations is $500 \times 600 \times 800$ mm for the X, Y, and Z axes, respectively. A representative result from the simulation is provided in Fig. 5b. It is found from the simulation that the conductive surface covered with aluminum is negatively charged by about -13 V relative to the ambient plasmas. In the simulation, the orbital speed of the satellite and the temperature of the ambient plasmas are 7.5 km/s and 0.2 eV, respectively. The plasma number density is $10^5/\text{cm}^3$. The positive ionic content of the plasma is oxygen. These plasma parameters in the simulation are consistent with the International Reference Ionosphere model. No magnetic field is included in the simulation.

In this simulation, a constant open circuit voltage is assumed for the solar arrays, whereas the short circuit current is assumed to be proportional to the intensity of incident sunlight. Note that because the power system of the satellite operates under peak power tracking (PPT) mode, the magnitudes of the actual output currents and voltages from the solar arrays are close to those

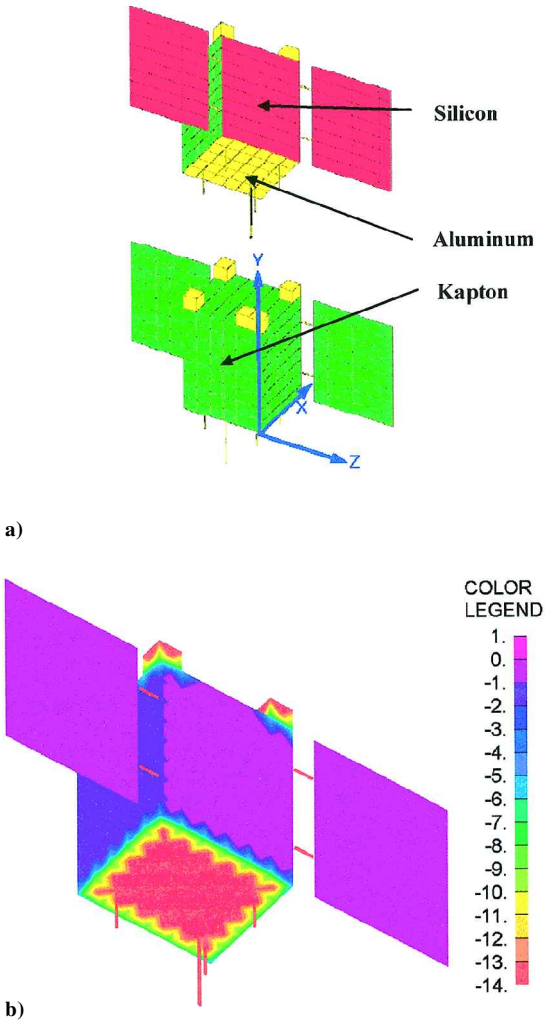

Fig. 5 Numerical simulation of KITSAT-3 with NASCAP/LEO: a) simulation model for KITSAT-3 and b) result from NASCAP/LEO.

of short circuit currents and open circuit voltages. Therefore, in the present simulation, the measured currents are employed as short circuit currents of the solar arrays. The open-circuit voltages are fixed in the simulation.

The space potentials in the $X-Z$ plane at $Y = 250$ mm are shown in Fig. 6 at points A, B, C, and D of Fig. 3. An obvious feature from the simulation is the slight negative charging of the wake of the satellite. Note that the orbital speed of the satellite is significantly greater than the thermal speed of positive ions. Therefore, a region of deficient positive ions should appear behind the orbital trajectory of the satellite. Consideration of current balance between the electrons and positive ions requires that the wake region should be charged negatively to attract positive ions and to repel electrons. It is interpreted that the negative charging of the wake region in Fig. 6 is due to the wake structure with deficient positive ions.[10,11]

Figure 7 summarizes the results of the simulation. The result shows that the floating potential of the satellite is initially about -13 V when the solar panels are directed toward the sun. Note again that the ETP instrument is saturated at -10 V, and any floating potentials smaller than -10 V will be detected by ETP at its saturation voltage. If the saturation is taken into account, a good agreement is found between the observation and simulations. Furthermore, it can be inferred from the simulation that the satellite is negatively biased by about -13 V when the solar arrays are sufficiently illuminated. The result is comparable to those of Sasaki[3] and Hastings et al.[4] for which negative charging of large space structures are investigated. Sasaki suggested that inward drift of ions during negative charging of SFU is responsible for the observed low-frequency fluctuations near 25 kHz. Theoretical investigation by Hastings et al.[4] also predicted large negative charging of the space station due to power generation of solar arrays. The present investigation finds that the effect of negative satellite charging is also found for a microsatellite satellite KITSAT-3.

Figure 8 shows space potentials near KITSAT-3 at points B and D of Fig. 3. The potentials in the $Y-Z$ plane at $X = 250$ mm are color-coded according to the color bar on the right-hand side of each plot. The dimension of the satellite along X axis is 500 mm. The UT for the simulation are chosen for attitudes A–E in Fig. 3. The maximum negative charging is represented in red and is found on the top and bottom conductive surfaces of the satellite. Inspection of

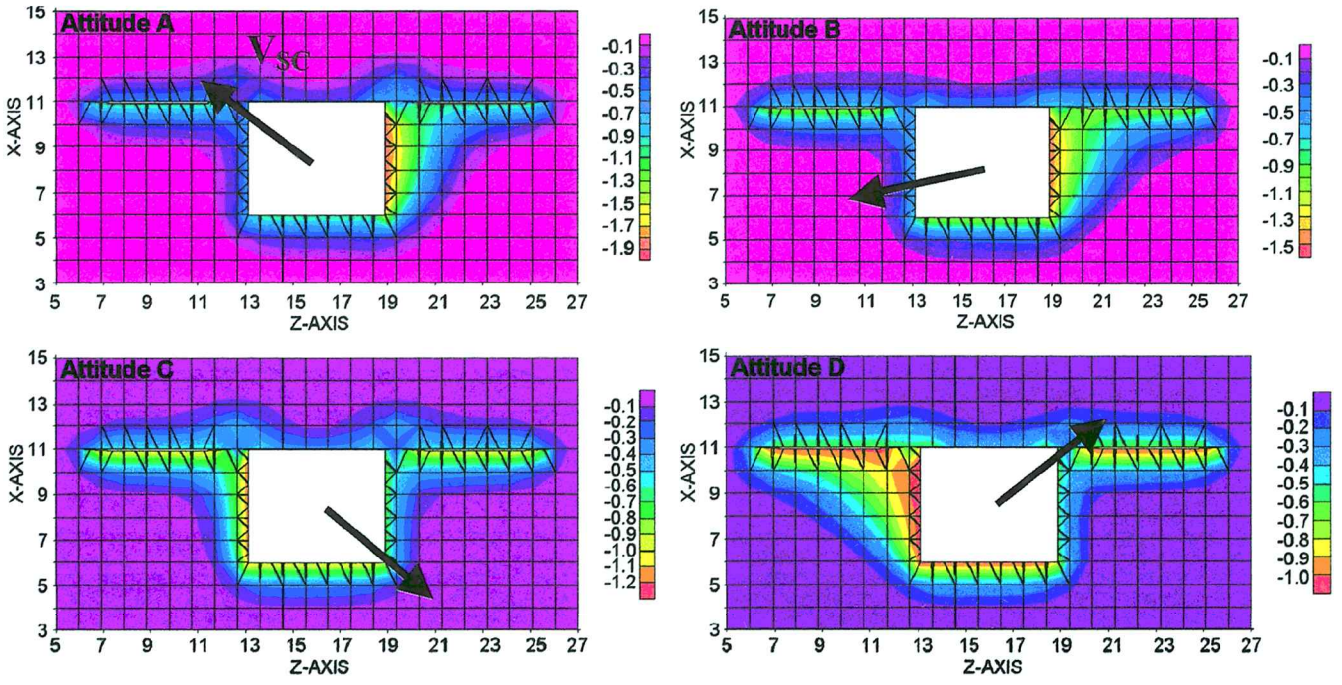

Fig. 6 Space potentials of KITSAT-3 in X–Z plane at $Y = 300$ mm for attitudes A, B, C, and D.

Fig. 3 allows an estimate that the conductive surface of the satellite is biased negative by the array by about −13, −3, −12, −6, and −13 V for points A, B, C, D, and E, respectively. The variation of the floating potentials for the conductive surfaces with respect to UT is demonstrated. Further comparisons of the simulation with the measurement from ETP can be found in Fig. 7.

The conductive area of solar cells by the presence of interconnectors between the solar cells is about $A_W \sim 270$ cm^2. A detailed layout of the solar array is shown in Fig. 9. On the other hand, the conductive area of the satellite body is about $A_C \sim 6100$ cm^2. Note that only the top and bottom surfaces of KITSAT-3 are covered with aluminum foil and are electrically connected to the satellite body. Therefore, only the top and bottom surfaces provide conductive areas. The rest of the satellite body surfaces are covered with Kapton. In the equilibrium situation, the collected ion currents from the negatively charged surfaces of the satellite body should balance any electron currents collected by the interconnectors. The method that was applied for the ISS by Hastings et al.[4] should also determine the potentials of KITSAT-3 as a function of

$$I = I_i(\Delta\Phi, \theta, A_w/A_c) + I_e(\Delta\Phi, \theta, A_w/A_c) \qquad (1)$$

where A_W/A_C is the ratio of the area of the interconnector with repect to the conductive area of the satellite body, respectively. I_i and I_e are currents by ions and electrons.

The simulation with NASCAP/LEO shows that the amount of currents collected by electron and positive ions is about 1×10^{-4} A. The ion current collected through satellite is the sum of I_{TH}(V) and I_{SC}. With a simplifying assumption that the shape of the satellite is spherical and that the sheath is thick, the following ion current for a spherical probe[12] is roughly obtained:

$$I_i = I_{TH} + I_{SC} \cong \left[\tfrac{1}{4}(1-\eta)v + \cos\alpha V_{SC}\right] neA_C$$

$$v = \sqrt{8kT/\pi m_i}, \qquad \eta = qV_p/kT \qquad (2)$$

where n, v, and A_s, are the plasma density, ion mean velocity, and surface area, respectively. Assumed values for n, T, A_s, and V_{sc} are 10^{11}/m^3, 0.2 eV, 5300 cm^2, and 7500 m/s, respectively. Because the angle α is close to 90 deg in the present analysis, the second term in Eq. (2) can be ignored. On the other hand, the calculated ion and electron currents from the NASCAP/LEO simulations are about 1.1×10^{-4} A. Setting the ion current to the calculated value in Eq. (2) yields a satellite potential about −8 V, which is in rough agreement with −13 V from NASCAP/LEO. This simple calculation demonstrates that the large negative biasing of the satellite is necessary for the current balance of the satellite.

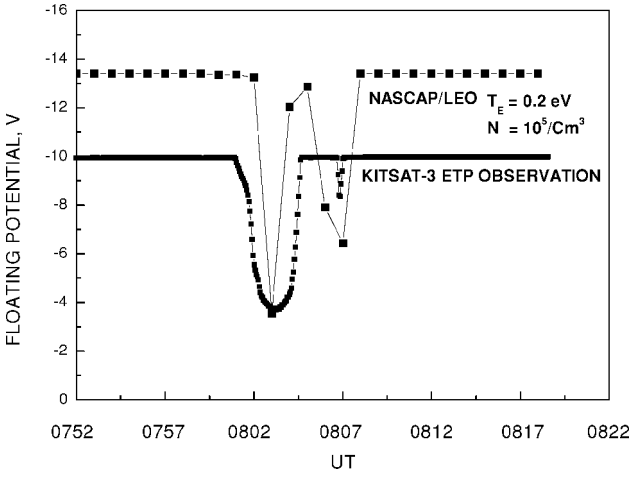

Fig. 7 Comparisons with observations and simulation.

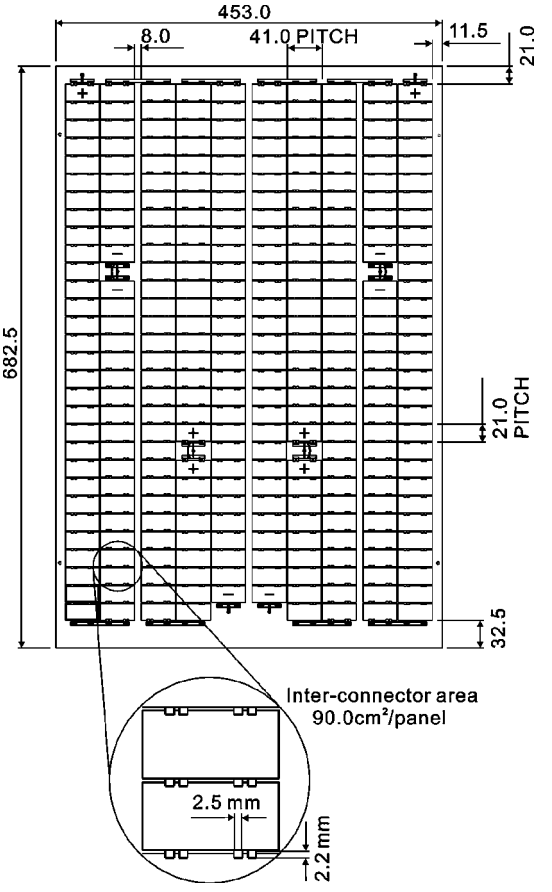

Fig. 9 Mechanical layout of solar arrays for KITSAT-3.

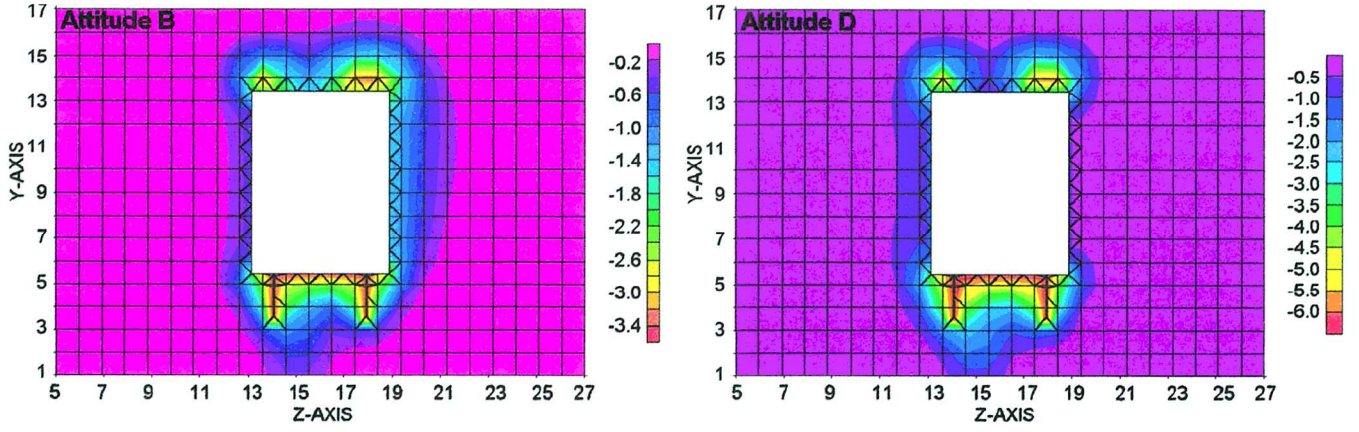

Fig. 8 Space potentials of KITSAT-3 in Y–Z plane at X = 250 mm for attitudes B and D.

Conclusions

A rotation of the microsatellite KITSAT-3 is performed in the dayside of the Earth. The electron temperature probe aboard the satellite measures large variations of floating potentials during the rotation. The variations are analyzed in terms of the negative charging of the satellite due to the presence of photovoltaic circuits in the solar arrays. A clear correlation between the floating potentials and the generated electric power from the solar arrays supports the interpretation. Additional numerical analysis further supports the interpretation and suggests that the satellite is negatively charged by about 13 V. Similar effects have been previously reported for large space structures. The present investigation finds that such negative charging of satellites is also present for a considerably smaller satellite, such as the microsatellite KITSAT-3.

Acknowledgments

This work was supported by Grant 1999-2-30600-001-3 from the Korea Science and Engineering Foundation. J. Seon is grateful to S. Sasaki, D. E. Hastings, M. Cho, and I. Katz for helpful discussions.

References

[1]Hastings, D. E., and Garrett, H., "Plasma Interactions," *Spacecraft-Environment Interactions*, 1st ed., Cambridge Univ. Press, New York, 1996, pp. 142–207.

[2]Langmuir, I., and Blodgett, K. B., "Currents Limited by Space Charge Between Concentric Spheres," *Physics Review*, Vol. 24, No. 1, 1924, pp. 49–59.

[3]Sasaki, S., "Plasma Effects Driven by Electromotive Force of Spacecraft Solar Array," *Geophysical Research Letters*, Vol. 26, No. 13, 1999, pp. 1809–1812.

[4]Hastings, D. E., Cho, M., and Wang, J., "Space Station Freedom Structure Floating Potential and the Probability of Arcing," *Journal of Spacecraft and Rockets*, Vol. 29, No. 6, 1992, pp. 830–834.

[5]Cho, M., Miyata, N., and Hikita, M., "Discharge over Spacecraft Insulator Surface in Low Earth Orbit Plasma Environment," *IEEE Transactions on Dielectrics and Electrical Insulation*, Vol. 6, No. 4, 1999, pp. 501–506.

[6]Shin, Y., Lee, D., Park, S., Lee, J., and Min, K., "Space Environment Scientific Experiment (SENSE) on KITSAT-3," *Proceedings of the Third Asia–Pacific Conference on Multilateral Cooperation in Space Technology and Applications*, Asia–Pacific Satellite Communications Council, Seoul, Republic of Korea, 1996, pp. 550–560.

[7]Oyama, K.-I., "Insitu Measurements of Te in the Lower Ionosphere—A Review," *Advances in Space Research*, Vol. 26, No. 8, 2000, pp. 1231–1240.

[8]Katz, I., Parks, D. E., Mandell, M. J., Harvey, J. M., Wang, S. S., and Roche, J. C., "NASCAP, a Three-Dimensional Charging Analyzer Program for Complex Spacecraft," *IEEE Transactions on Nuclear Science*, Vol. 24, No. 6, 1977, pp. 2276–2280.

[9]Mandell, M. J., and Davis, V. A., *User's Guide to NASCAP/LEO* (Draft), SSS-R-85-7300-R2, S-Cubed Div. of Maxwell Labs., Inc., 1990, pp. 6-1, 10-1.

[10]Samir, U., and Willmore, A. P., "The Distribution of Charged Particles Near a Moving Spacecraft," *Planetary and Space Science*, Vol. 13, No. 4, 1965, pp. 285–296.

[11]Samir, U., and Wrenn, G. L., "The Dependence of Charge and Potential Distribution Around a Spacecraft on Ionic Composition," *Planetary and Space Science*, Vol. 17, No. 4, 1969, pp. 693–706.

[12]Lochte-Heltgreven, W., "Electrical Probes," *Plasma Diagnostics*, North-Holland, Amsterdam, 1968, pp. 675–681.

D. L. Cooke
Associate Editor